



HAL
open science

H 1 -parameterizations of plane physical domains with complex topology in Isogeometric analysis

Meng Wu, Bernard Mourrain, André Galligo, Boniface Nkonga

► **To cite this version:**

Meng Wu, Bernard Mourrain, André Galligo, Boniface Nkonga. H 1 -parameterizations of plane physical domains with complex topology in Isogeometric analysis. 2015. hal-01196435v1

HAL Id: hal-01196435

<https://inria.hal.science/hal-01196435v1>

Preprint submitted on 9 Sep 2015 (v1), last revised 26 Apr 2017 (v3)

HAL is a multi-disciplinary open access archive for the deposit and dissemination of scientific research documents, whether they are published or not. The documents may come from teaching and research institutions in France or abroad, or from public or private research centers.

L'archive ouverte pluridisciplinaire **HAL**, est destinée au dépôt et à la diffusion de documents scientifiques de niveau recherche, publiés ou non, émanant des établissements d'enseignement et de recherche français ou étrangers, des laboratoires publics ou privés.

H^1 -parameterizations of plane physical domains with complex topology in Isogeometric analysis

Meng Wu* Bernard Mourrain André Galligo
Boniface Nkonga

School of Mathematics, Hefei University of Technology, P. R. China.
Galaad, Inria, Sophia Antipolis, France
Lab. J. A. Dieudonné, University of Nice, Nice, France

Abstract

Isogeometric analysis (IGA) is a method for solving geometric partial differential equations(PDEs). Generating parameterizations of a PDE's physical domain is the basic and important issues within IGA framework. In this paper, we present a global H^1 -parameterization method for a planar physical domain with complex topology.

1 Introduction

IGA method was proposed by Hughes et al. [1] to bridge the gap between the geometry description of the physical domain and numerical analysis. Within IGA framework, the same basis functions are used to describe physical domains and IGA solutions obtained by numerical analysis.

A map to describe physical domains is called a parameterization of this physical domain in IGA framework. The parameterization of the physical domain has an impact on the simulation result, the efficient of the computation and the stability of numerical system[2],[3],[4]. Until now, there is no simple standard for measuring the quality of parameterization. In this paper, we develop a method for modifying the initial parameterization focused on three basic requirements.

Firstly, for describing the geometry of physical domains, parameterizations should be no self-intersection such as [5],[6], [7]. In other words, it is an injective map.

*M. Wu (Corresponding author, email: meng.wu@hfut.edu.cn), B. Mourrain (email: Bernard.Mourrain@inria.fr), A. Galligo(email: Andre.Galligo@unice.fr), B. Nkonga (email: Boniface.Nkonga@unice.fr)

Secondly, for numerical analysis, the condition number of the linear system obtained within IGA framework should be as small as possible [8, 9]. Smaller condition numbers bring the efficiency and numerical stability. In application, this linear system is always a large size. It is better to use iteration solvers in order to reduce the computation costs. At that moment, smaller condition number means rapid convergence and more accurately linear system solution. However, the condition number of the linear system in IGA depends on the underlying parameterization. Thus, we expect to obtain a parameterization which will bring a smaller condition number of the linear system within IGA framework.

Thirdly, the regularity property of test functions on physical domains is considered. The test functions used in Galerkin based IGA are obtained by composing the inverse of the parameterization with basis functions used in IGA. Thus, the algorithm of generating parameterizations has impacted on the regularity property of test functions on physical domains. For example, in papers [19, 20], the singularity of parameterizations should satisfy some additional conditions which guarantee the regularity properties of test functions on physical domains.

In this paper, based on these three requirements, we develop an algorithm for modifying the quality of initial parameterizations with fix boundary representation. The resulting parameterization, called H^1 -parameterization, satisfies H^1 integral assumption in [19] for solving second order PDEs, such as the Grad-Shafranov equation which is the equilibrium in the resistive magneto hydrodynamic model. This algorithm can be applied to several situations, which is stated in Section 3.3. Usually, Non-Uniform Rational B-Splines (NURBS) are treated as basis functions of the classical IGA, i.e. NURBS-based IGA. However, when we consider the planar physical domain with complex topology, patching multiple NURBS parameterizations or trimming techniques, such as [10], has to be considered. To obtain a global representation of physical domains with complex geometry features and topology features, in this paper, the bicubic splines with rigid transformations in [11] are used to represent the global parameterizations.

This paper is structured as follows. In Section 2, the global parameterization is introduced and some properties of this parameterization will be presented. Then, taking into account these properties, we develop the modification algorithm for initial parameterizations in Section 3. By this algorithm, in Section 4, several experiments are presented to modify the initial parameterizations of physical domains with geometric features (such as sharp corners and non-convex shapes) or topology features (such as a lot of holes inside). In Section 5, We conclude this paper with future work directions. At last, all the proofs of lemmas or theorems are collected in Section 6 as the appendix of this paper.

2 Parameterization with splines defined over meshes with complex topologies

In this paper, C^1 splines with complex topology is used to represent this parameterization in order to give a global parameterization even if the physical domain with complex topology. In order to avoid the complicated definitions, in this section, the intuitive explanation of this type of splines is presented. One can refer to [11] for their mathematical definitions. Based on this intuitive explanation, the parameterization represented by these splines is decomposed into two parts. The different modification algorithms for these two parts will be presented in Section 3 later.

2.1 Introduce an intuitive explanation of splines

Before introducing the splines, parametric meshes are presented because the splines are defined over this type of mesh.

The concept of parametric meshes in this paper is generalized from the classical tensor product meshes. In Figure 1, there is a 2D tensor product mesh which contains anisotropic rectangles with arbitrary aspect ratio. These rectangles are known as the cells of this 2D tensor product mesh and these grid points are called its vertices. In order to obtain a global parameterization without trimming of surfaces with more complex topology such as surfaces with holes inside or sphere, we generalize the concept of 2D tensor product mesh to the parametric mesh.

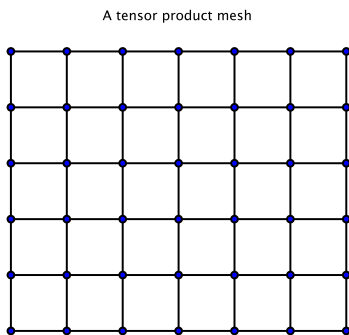


Figure 1: A 2D tensor product mesh

By relaxing the restrictions of the degree of each vertex, parametric meshes in this paper contain more complex topology meshes. For example, in Figure 2, there are some undirected graphs \mathcal{M}_t which share the same topology with corresponding parametric meshes \mathcal{M} . From the view of topology, we make no difference between \mathcal{M} and \mathcal{M}_t (denoted as \mathcal{M} as well).

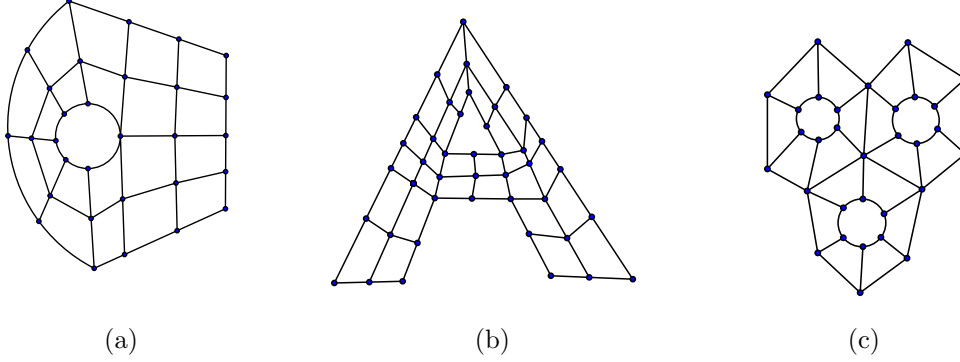


Figure 2: Examples of the topology of parametric meshes (\mathcal{M} s)

In the following, we will introduce some concepts. Take \mathcal{M} in Figure 3(a) for example. $\{v^i : i = 1, 2, \dots, 10\}$ and $\{v_b^j : j = 1, 2, \dots, 20\}$ are vertices of \mathcal{M} . Here $v_b^j (j = 1, 2, \dots, 20)$ are **boundary vertices** and $v^i (i = 1, 2, \dots, 10)$ are **interior vertices**. The degree of a vertex of undirected graph \mathcal{M} is referred to as the valence of this vertex. If the degree of interior vertex is not 4, this vertex is **irregular**, which is called the extraordinary vertex. Other vertices are **regular**. An edge of \mathcal{M} is used to connect adjacent vertices. In Figure 3(a), $v_b^{15}v_b^{20}, v^1v^2, v^1v_b^1$ are edges of \mathcal{M} . Here, $v_b^{15}v_b^{20}$ is a **boundary edge** of \mathcal{M} . $v^1v^2, v^1v_b^1$ are interior edges. Quadrilaterals with curves edges are treated as cells of \mathcal{M} such as $v_b^{15}v_b^{20}v^{10}v^1, v^3v^4v_b^{18}v_b^{17}$ and $v_b^5v_b^6v^6v^5$.

A local frame of a cell C : Owing to the topology of the parametric mesh, for each cell of the parametric mesh, a local frame is introduced. For example, in Figure 3(a), $\{\mathbf{s}_C, \mathbf{t}_C\}$ is a local frame of the cell C .

Local parameters of a cell C : Based on the local frame of a cell, this spline can be described with local parameters over each cell. For example, in Figure 3(a), the local parameters of the cell C are denoted as (s_C, t_C) . Associated to these local parameters, the splines used in this paper is a bicubic polynomial over a cell and with C^1 continuity globally.

Associated with each vertex of \mathcal{M} , splines will be introduced to represent parameterizations in the following context. Based on the different types of vertices, splines will be classified into two classes.

1. For an extraordinary vertex v_{ir} , there is a spline $B_{v_{ir}}^p$ defined at v_{ir} . Its coefficient $\mathbf{P}_{v_{ir}} \in \mathbb{R}^2$ stands for the position of v_{ir} . This spline is called the **position spline** of v_{ir} .
2. For a regular vertex v_r , three splines $B_{v_r}^p, B_{v_r}^s$ and $B_{v_r}^t$ will be defined over \mathcal{M} . For $B_{v_r}^p$, its coefficient $\mathbf{P}_{v_r} \in \mathbb{R}^3$ stands for the position of v_r . $B_{v_r}^p$ is called the position spline of v_r . $B_{v_r}^s$ and $B_{v_r}^t$ are called **tangent splines**.

In order to explain the coefficients of $B_{v_r}^s$ and $B_{v_r}^t$, the local frame attached to v_r is introduced. This local frame $(\mathbf{s}_{v_r}, \mathbf{t}_{v_r})$ is the same as one of the local frames

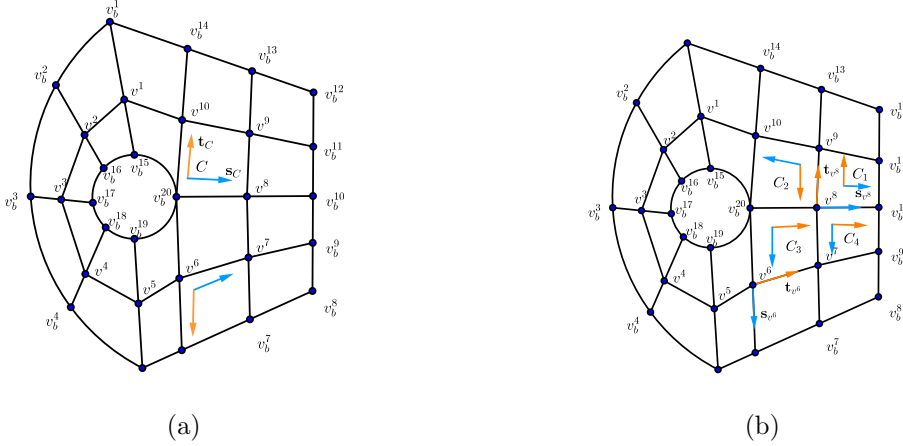


Figure 3: An example of \mathcal{M} for introducing the concepts of parametric meshes.

of the cells around v_r . For example, in Figure 3(b), at v^8 , there is a local frame $(\mathbf{s}_{v^8}, \mathbf{t}_{v^8})$ which is the same as the local frame of C_1 . $\mathbf{T}_{v_r}^s$ (or $\mathbf{T}_{v_r}^t$) is the tangent vector of the s -curve (or t -curve) at v_r , where s -curve (or t -curve) means the image of mesh grid line of parameterization along \mathbf{s}_{v_r} (or \mathbf{t}_{v_r}) direction. For example, in Figure 4(b), the domain is an image of one of parameterizations defined over \mathcal{M} shown in Figure 4(a). By this parameterization, s -curve is consisting of the image of the edges $v_b^{20}v^8, v^8v_b^{10}$ of the direction which is matching with the local frame \mathbf{s}_{v^8} attached to v^8 . Similarly, t -curve can be defined.

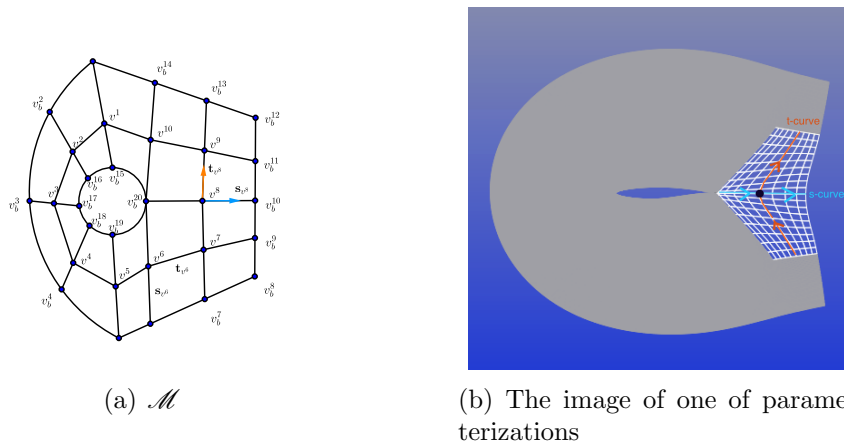
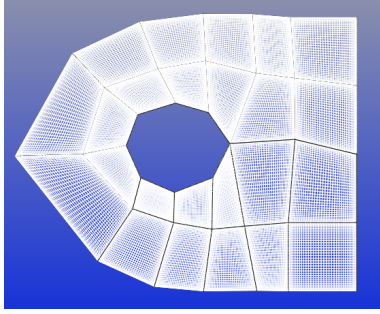


Figure 4: s -curve and t -curve at v^8

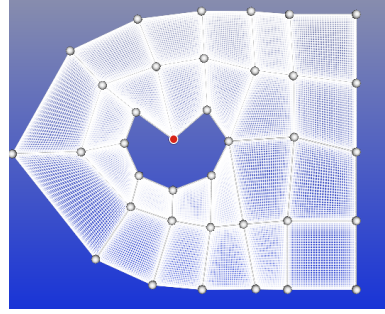
Based on these splines, the parameterization is constructed as a linear combination of these splines,

$$\mathcal{P} = \sum_{v \in V} \mathbf{P}_v B_v^p + \sum_{v_r \in V_r} (\mathbf{T}_{v_r}^s B_{v_r}^s + \mathbf{T}_{v_r}^t B_{v_r}^t) \quad (1)$$

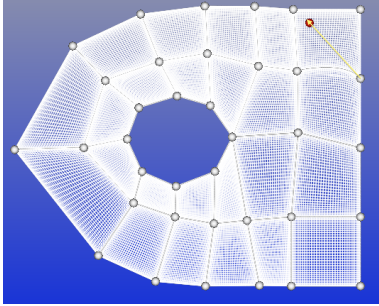
where V and V_r are the set of vertices and the set of regular vertices of \mathcal{M} . In this paper, parameterizations of a planar physical domain are considered, i.e. $\mathbf{P}_v, \mathbf{T}_{v_r}^s, \mathbf{T}_{v_r}^t \in \mathbb{R}^2$. For example, Figure 5(a) is the original parameterization. In Figure 5(b), by changing \mathbf{P}_v of the given vertex, the position of this vertex is changed. In Figure 5(c) and Figure 5(d), by setting $\mathbf{T}_{v_r}^s$ and $\mathbf{T}_{v_r}^t$, the parameterization has been changed around this vertex.



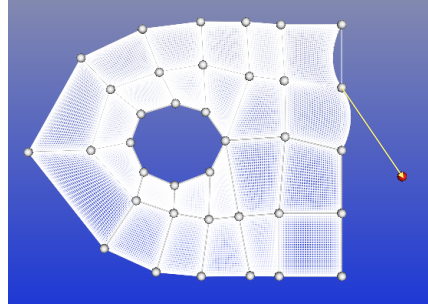
(a) The original parameterization



(b) Changing \mathbf{P}_v of the original parameterization in Figure 5(a) at the given vertex



(c) Changing \mathbf{T}_v^s or \mathbf{T}_v^t of the original parameterization in Figure 5(a) at the given vertex



(d) Changing \mathbf{T}_v^s or \mathbf{T}_v^t of the original parameterization in Figure 5(a) at the given vertex

Figure 5: The meaning of coefficients of splines defined over the parametric mesh in Figure 3(a)

Jacobian of \mathcal{P} : Let p be a point of \mathcal{M} , then there is a cell C of \mathcal{M} such that $p \in C$. Consider $\mathcal{P}|_C$, by Equation (1), $\mathcal{P}|_C = (x(s_C, t_C), y(s_C, t_C))$, where $x(s_C, t_C), y(s_C, t_C)$ are bicubic polynomials. Thus the Jacobian of \mathcal{P} at p is

$$\begin{vmatrix} \frac{\partial x(s_C, t_C)}{\partial s_C} & \frac{\partial x(s_C, t_C)}{\partial t_C} \\ \frac{\partial y(s_C, t_C)}{\partial s_C} & \frac{\partial y(s_C, t_C)}{\partial t_C} \end{vmatrix}_p$$

2.2 Parameterizations of planar physical domains

In this section, we will analyze the parameterization represented by the splines defined in Section 2.1. Based on the meaning of coefficients of each spline, the parameterization \mathcal{P} can be decomposed into two parts \mathcal{P}_p and \mathcal{P}_t . i.e.,

$$\mathcal{P} = \mathcal{P}_p + \mathcal{P}_t,$$

where $\mathcal{P}_p = \sum_{v \in V} \mathbf{P}_v B_v^p$, $\mathcal{P}_t = \sum_{v_r \in V_r} (\mathbf{T}_{v_r}^s B_{v_r}^s + \mathbf{T}_{v_r}^t B_{v_r}^t)$. \mathbf{P}_v is the position coordinates of the vertex v . $\mathbf{T}_{v_r}^s$ and $\mathbf{T}_{v_r}^t$ are the tangent vectors of the s -curve and t -curve at v_r .

\mathcal{P}_p : For this part of parameterization, the coefficients of the position splines are the positions of vertices in the physical domain. Thus, modifying \mathcal{P}_p equals to find a method to distribute the layout of an undirected graph [13, 14]. This modification algorithm will be dealt with in Section 3.1. Take the parameterization presented in Figure 5(a) for example. This parameterization is only represented by the position splines at each vertex, i.e. the coefficients of $\mathbf{T}_{v_r}^s, \mathbf{T}_{v_r}^t$ are zeros. In Figure 6, the Jacobian of the parameterization shown in Figure 5(a) has been put forward. From the view of Jacobian, Jacobian along the s -curves and t -curves is zero. Generally,

Lemma 2.1. *Jacobian of \mathcal{P}_p is zero along s -curves and t -curves at any vertex of \mathcal{M} .*

This lemma will be proved in Section 6. It is necessary to add an non-trivial \mathcal{P}_t in order to get a parameterization with a better Jacobian.

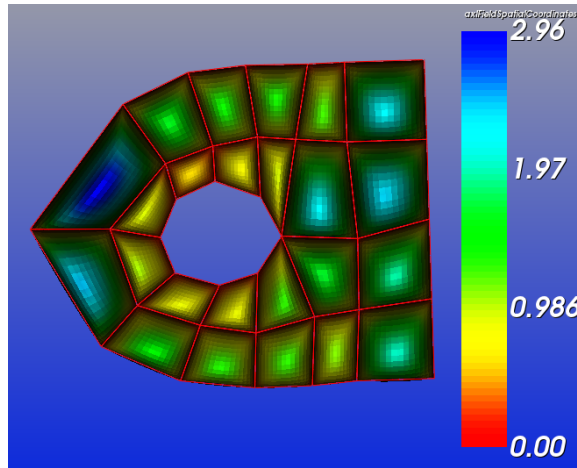
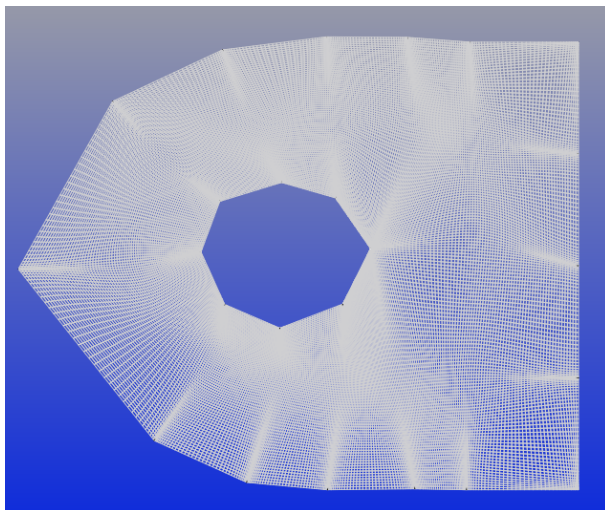


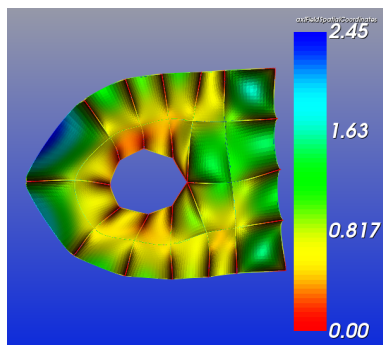
Figure 6: Jacobian of the parameterization in Figure 5(a)

\mathcal{P}_t : By adding an non-trivial \mathcal{P}_t , Jacobian of \mathcal{P} will be modified from the original \mathcal{P}_p , where $\mathcal{P} = \mathcal{P}_p + \mathcal{P}_t$. For example, by adding an non-trivial \mathcal{P}_t at the interior vertices of \mathcal{M} shown in Figure 7(c), the parameterization is shown in Figure 7(a)

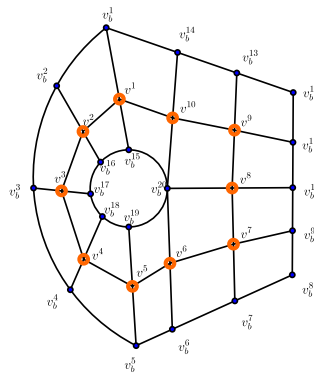
instead of the one shown in Figure 5(a). By the way, Jacobian of the parameterization shown in Figure 7(a) has been demonstrated in Figure 7(b). By comparing the parameterizations shown in Figures 5(a) and 7(a), the parameterization becomes smoothing after adding an non-trivial \mathcal{P}_t at interior regular vertices. We will develop an algorithm in Section 3.2 called the smoothing algorithm for choosing a suitable \mathcal{P}_t at the regular interior vertices of the parametric mesh.



(a) The parameterization after adding an non-trivial \mathcal{P}_t at the regular interior vertices of the parameterization shown in Figure 5(a)



(b) Jacobian of the parameterization after adding an non-trivial \mathcal{P}_t at the regular interior vertices of the parameterization shown in Figure 5(a)



(c) The parametric mesh and its regular interior vertices marked in red

Figure 7: Change the coefficients of tangent splines at the regular interior vertices

3 The parameterization Algorithm

In this section, suppose an initial parameterization \mathcal{P}_0 is given. We will develop an algorithm to modify \mathcal{P}_0 with fixed boundaries such that the resulting parameterization satisfies the three requirements in Introduction, i.e. an injective map, smaller condition numbers and H^1 -parameterization. Based on the analyzing in Section 2.2, \mathcal{P}_0 can be decomposed into two parts. For modifying \mathcal{P}_0 , there are two steps matching with these two parts. The first step equals to distribute the layout of an undirected graph with fixed boundaries, in other words, determining the position splines of the coefficients at interior vertices. A force-directed layout algorithm is presented in Section 3.1; The second step is the smoothing algorithm which is used to modifying the tangent splines' coefficients at each interior regular vertex in Section 3.2. In Section 3.3, applications of this generating parameterization algorithm are presented.

3.1 The force-directed layout algorithm

Force-directed algorithms are among the most flexible methods for calculating layouts of simple undirected graphs. These force-directed algorithms tend to be aesthetically pleasing way, exhibit symmetries and tend to produce crossing-free layouts for planar graphs. The first graph drawing algorithm [16] is a force-directed method. In this section, we will deal with layout of the undirected graph with fixed boundaries based on the spring model and the point-charge model. This undirected graph is given by the image of the vertices and edges of the parameter mesh. Then, the position splines' coefficients of interior vertices are re-determined.

In order to re-display the vertices, the following energy is presented. Let $P_i(t)$ be the position according to $v_i \in V^o$ ($i = 1, 2, \dots, n$) and $P_i(t)$ evolves with time.

$$E(P_1(t), P_2(t), \dots, P_n(t)) = \sum_{v_i \in V^o} \|k\mathbf{F}_i^{sp}(t) + \mu\mathbf{F}_i^{ch}(t)\|_{L_2}, \quad (2)$$

where k and μ are parameters of this model, $\mathbf{F}_i^{sp}(t) = \sum_{P_j(t) \in N^1(P_i(t))} \overrightarrow{P_i(t)P_j(t)}$ and $\mathbf{F}_i^{ch}(t) = \int_{P \in \partial\Omega} \overrightarrow{P_i(t)P} / (\|\overrightarrow{P_i(t)P}\|_{L_2})^2 ds$. V^o is the set of interior vertices of \mathcal{M} . Ω is the physical domain. For \mathbf{F}_i^{sp} , it is from the spring force at $P_i(t)$. And $\mathbf{F}_i^{ch}(t)$ describes the electric force from $\partial\Omega$ to $P_i(t)$. Suppose $\partial\Omega, P_i(t)$ carry the same type of charges. By the definition of $\mathbf{F}_i^{ch}(t)$, when $P_i(t)$ closes to the boundary of Ω , $\mathbf{F}_i^{ch}(t)$ becomes large. Thus, $P_i(t)$ is confined within $\partial\Omega$ if the initial position of $P_i(t)$ is within Ω and $\mu > 0$.

In order to develop the force-directed algorithm to minimize $E(P_1(t), P_2(t), \dots, P_n(t))$, there is a lemma.

Lemma 3.1. *Suppose that the velocity of $P_i(t)$ at t_0 is $\mathbf{0}$. Then*

$$P_i(t_0 + \Delta t) - P_i(t_0) = \frac{\mathbf{F}_i(t_0)\Delta t^2}{2m_i} + o(\Delta t^2).$$

where $\mathbf{F}_i(t_0) = \mathbf{F}_i^{sp}(t_0) + \mathbf{F}_i^{ch}(t_0)$.

This lemma will be proved in Section 6. Based on this lemma, the new position of $P_i(t)$ at $t_0 + \Delta t$ can be given by

$$P_i(t_0 + \Delta t) - P_i(t_0) = \Delta P_i(t_0) \approx \frac{\mathbf{F}_i(t_0)\Delta t^2}{2m_i}. \quad (3)$$

Thus we can choose a suitable time step Δt and the parameters such as m_i, k, μ . The new position of $P_i(t_0 + \Delta t)$ after one iteration can be approximated by $P_i(t_0) + \Delta P_i(t_0)$.

By analysing, now the algorithm is provided in the following. Set the parameters $\epsilon_0, \Delta t, k, \mu$ and *MaxIterNumber*, where ϵ_0 is the parameter employed to judge this algorithm converges or not. Δt is the time step. k and μ are the parameters shown in Equation (2). *MaxIterNumber* is the maximum number of iteration of this algorithm.

Algorithm 1 Local Reducing Energy Algorithm

Require: Input the original positions of all the points P_i , the parametric mesh \mathcal{M} , $\epsilon_0, \Delta t, k$ and μ . Set $m_i = 1, \epsilon = \epsilon_0 + 1$ and *IterationNum* = 0.

Ensure:

```

while ( $\epsilon > \epsilon_0$ ) && (IterationNum < MaxIterNumber) do
   $\epsilon \leftarrow 0$ 
  IterationNum  $\leftarrow$  IterationNum + 1
  for all  $P_i$  which is the image of an interior vertex if  $\mathcal{M}$  do
    Compute  $\Delta P_i$  based on Equation (3)
     $\epsilon \leftarrow \epsilon + \|\Delta P_i\|_{L_2}$ 
     $P_i \leftarrow P_i + \Delta P_i$ 
  end for
   $\epsilon \leftarrow \epsilon / \#\{P_i\}$ 
end while

```

In this algorithm, ϵ is a parameter used to store the average of the relative distance of all of interior P_i for each iteration. If ϵ is small enough, $\{P_i\}$ should be in a balance state, i.e., if $\epsilon < \epsilon_0$, this algorithm converges. $\#\{P_i\}$ is the number of the interior vertices of \mathcal{M} .

3.2 The Smoothing Algorithm

Based on Algorithm 1, at the interior vertices, the position splines' coefficients have been obtained. In this section, a method for determining the coefficients of tangents splines at interior regular vertices is presented. Due to subdivision process of the mesh, suppose that all the extraordinary vertices. In the following, there is an observation.

Theorem 3.2. *Let \mathcal{M} be a parametric mesh and C is one of its cells. Suppose that $C = [0, 1] \times [0, 1]$ and its local parameters are (s, t) . Denote its corners $(0, 0), (1, 0), (1, 1), (0, 1)$ as v_1, v_2, v_3, v_4 respectively. If the images of v_1, v_2, v_3, v_4 of a parameterization are P_1, P_2, P_3, P_4 and P_1, P_2, P_3, P_4 are form a convex quadrilateral. Then,*

- if v_1, v_2, v_3, v_4 are regular vertices of \mathcal{M} , $\mathbf{T}_{v_1}^s = \mathbf{T}_{v_2}^s = \overrightarrow{P_1P_2}$, $\mathbf{T}_{v_1}^t = \mathbf{T}_{v_4}^t = \overrightarrow{P_1P_4}$, $\mathbf{T}_{v_3}^t = \mathbf{T}_{v_2}^t = \overrightarrow{P_2P_3}$, $\mathbf{T}_{v_3}^s = \mathbf{T}_{v_4}^s = \overrightarrow{P_4P_3}$;
- if there is a vertex, supposing v_1 , is an extraordinary vertex of \mathcal{M} , $\mathbf{T}_{v_2}^s = \overrightarrow{P_1P_2}$, $\mathbf{T}_{v_4}^t = \overrightarrow{P_1P_4}$, $\mathbf{T}_{v_3}^t = \mathbf{T}_{v_2}^t = \overrightarrow{P_2P_3}$, $\mathbf{T}_{v_3}^s = \mathbf{T}_{v_4}^s = \overrightarrow{P_4P_3}$

then \mathcal{P} is injective over C and it satisfies H^1 integral assumption.

In the following, we start to set the coefficients of tangent splines in general case. Let v_i be a regular interior vertex of \mathcal{M} and its position has been determined by Algorithm 1. There are four cells which take v_i as their corner vertex since v_i is regular. Based on Lemma ?? over a cell, the tangents at this regular vertex v_i are estimated by $P_i, P_i^1, P_i^2, P_i^3, P_i^4$, where $P_i = \mathcal{P}(v_i)$ and $N^1(P_i) = \{P_i^1, P_i^2, P_i^3, P_i^4\}$ shown in Figure 8, where C_1, C_2, C_3, C_4 are cells around v_i .

If C_1, C_2, C_3, C_4 have the same local frame and $C_i = [0, 1] \times [0, 1]$, the tangent vectors at v_i can be taken as an average of the coefficients given by Lemma ?? when we consider these coefficients cell by cell, i.e.,

$$\mathbf{T}_{v_i}^s = 1/2\overrightarrow{P_iP_i^2} + 1/2\overrightarrow{P_iP_i^4}; \quad \mathbf{T}_{v_i}^t = 1/2\overrightarrow{P_iP_i^1} + 1/2\overrightarrow{P_iP_i^3}, \quad (4)$$

Generally, C_1, C_2, C_3, C_4 can have different local frames, if the direction of s -curve of v_i is along $P_iP_i^2$ and the direction of t -curve at v is along $P_iP_i^1$, then

$$\mathbf{T}_{v_i}^s = \frac{1}{2\ell_1}\overrightarrow{P_iP_i^4} + \frac{1}{2\ell_2}\overrightarrow{P_iP_i^2}; \quad \mathbf{T}_{v_i}^t = \frac{1}{2\ell_3}\overrightarrow{P_iP_i^3} + \frac{1}{2\ell_4}\overrightarrow{P_iP_i^1}.$$

where ℓ_1 is the distance between v_i^4 and v_i considered in C_4 , ℓ_2 is the distance between v_i and v_i^2 considered in C_1 , ℓ_3 is the distance between v_i^3 and v_i considered in C_2 , ℓ_4 is the distance between v_i and v_i^1 considered in C_1 . Discuss how to select $\mathbf{T}_{v_i}^s, \mathbf{T}_{v_i}^t$ in the other cases of the local frame at v_i similarly. Now, the smoothing algorithm can be presented.

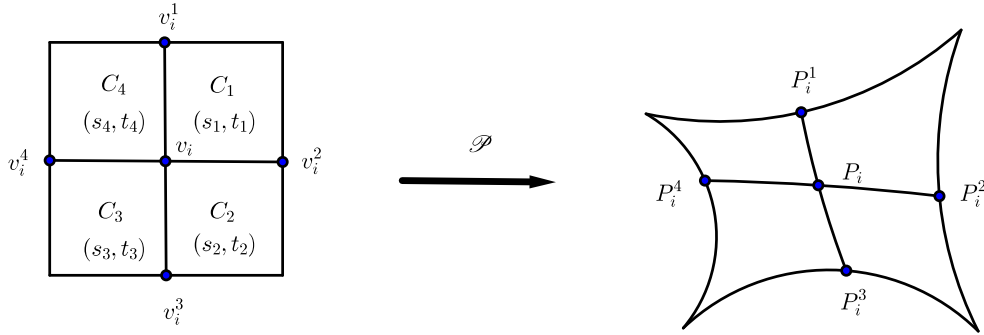


Figure 8: The interior regular vertex P_i and $N^1(P_i) = \{P_i^1, P_i^2, P_i^3, P_i^4\}$

Algorithm 2 The Smoothing Algorithm

Require: Input \mathcal{M} , \mathcal{P}_1 generated from the initial parameterization \mathcal{P}_0 by Algorithm 1 and $\{P_i\}$ which are the resulting positions by Algorithm 1.

Ensure:

for $\{P_i\}$ **do**

if v_i is an interior regular vertex **then**

 Compute P_i 's 1-neighbourhood $N^1(P_i)$ based on the topology of \mathcal{M}

 Determine $\mathbf{T}_{v_i}^s$ and $\mathbf{T}_{v_i}^t$ by the method presented in this section, where v_i is the vertex corresponding to P_i .

else

$\mathbf{T}_{v_i}^s, \mathbf{T}_{v_i}^t$ inherit from \mathcal{P}_0 .

end if

end for

3.3 Applications of the generating parameterization algorithm

In order to simulate the two-dimensionality of the flow over the RAE2822 airfoil, the physical domain is a bounded domain around it. The initial parameterization is produced by fitting the sample points of its boundary. Thus, during modification the initial parameterization, fixing boundaries are expected.

In this section, a bounded planar physical domain over the RAE2822 airfoil will be parameterized by the algorithm developed in Sections 3.1 and 3.2. Here the topology of the parametric mesh \mathcal{M} is shown in Figure 9. The inside boundary which has been marked in red in Figure 9 of this physical domain should fit the sample points shown in Figure 10(a). After fitting, we get the initial parameterization of this physical domain shown in Figure 10(b).

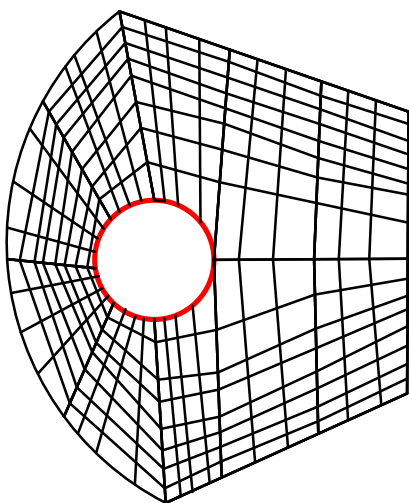
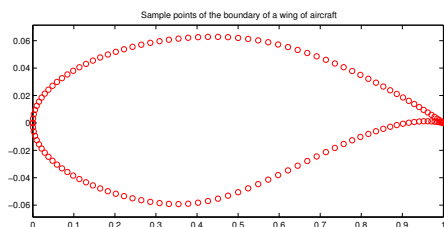
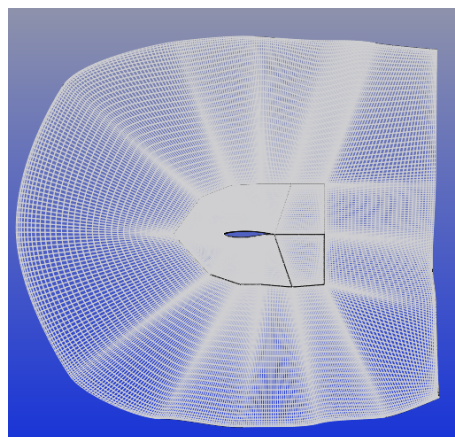


Figure 9: The topology of the parametric mesh in the example in Section 3.3



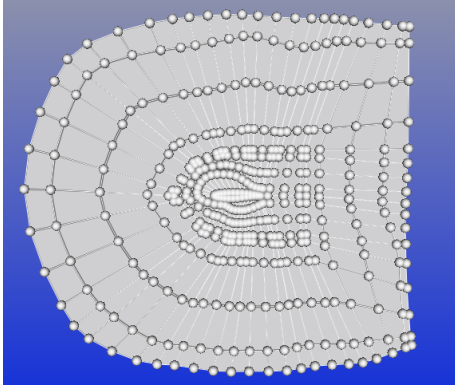
(a) The sample points from the RAE2822 airfoil



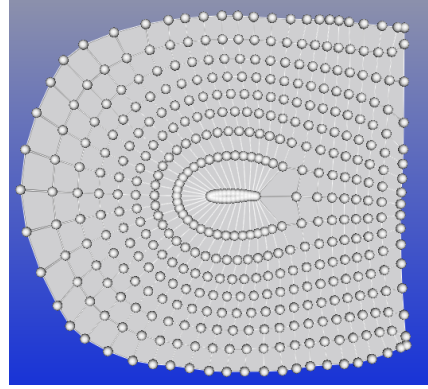
(b) The initial parameterization of the physical domain

Figure 10: The sample points and the initial parameterization by fitting

Before using Algorithm 1, the layout of the position vertices of the initial parameterization is illustrated in Figure 11(a). Take $k = 1, \mu = 0.01, \Delta t = 0.5$, after 100 iterations, the layout of position vertices of resulting parameterization is shown in Figure 11(b).



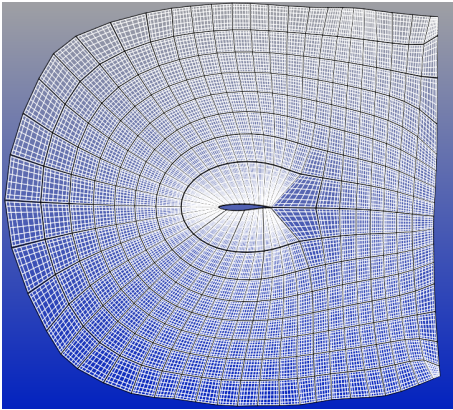
(a) The layout of vertex positions of the initial parameterization



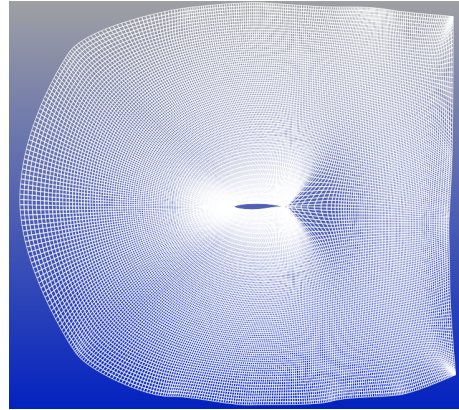
(b) The layout of vertex positions modified by Algorithm 1

Figure 11: Apply Algorithm 1 to the example in Section 3.3

Thus we can get a parameterization of the physical domain with the new position of vertices shown in Figure 12(a). Then, by Algorithm 2, at each regular interior vertex, the tangent splines' at coefficients are modified. At this moment, we get the resulting parameterization presented in Figure 12(b).



(a) The parameterization given by the position of vertices after using Algorithm 1



(b) Adding the tangents information to the parameterization shown in Figure 12(a) by Algorithm 2

Figure 12: Apply Algorithm 2 to the example in Section 3.3

In Figures 13(a) and 13(b), Jacobians of the parameterizations shown in Figures 12(a) and 12(b) are compared.

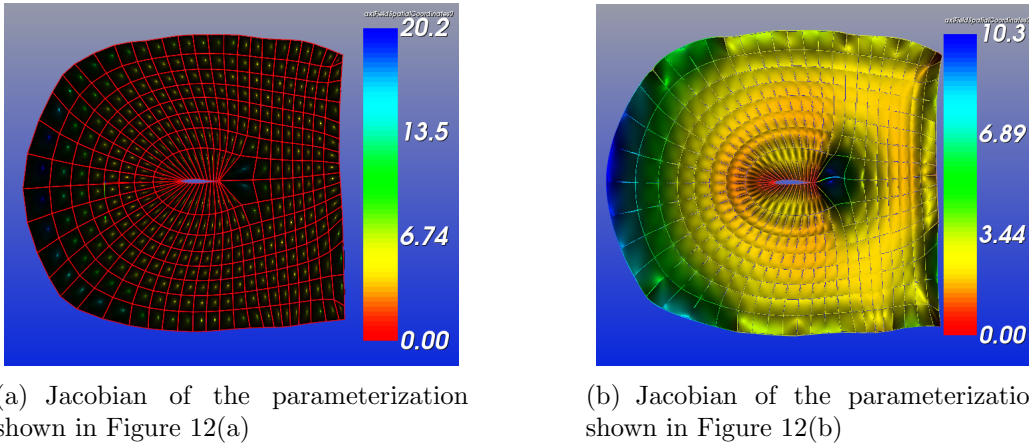


Figure 13: Jacobians of the parameterizations before applying Algorithm 2 and after Algorithm 2

Another application of the algorithm developed in this paper appears in solving PDE within IGA framework. After h-refinement, updating the initial parameterization is expected to obtain a better approximation of the physical domain and a smaller condition number of the linear system within IGA framework. Because more degree of freedoms are generated after h-refinement of the parametric mesh. A better boundary approximation yields a better approximation of the physical domain. A smaller condition number of the linear system, which brings rapid convergence of iteration solvers and more accurately linear system solution, is determined by the quality of parameterization within the inner of the physical domain. Logically, after updating the boundary approximation, the quality of parameterization within the inner of the physical domain is considered. Thus, fixing boundary representation is necessary during improving the quality of parameterization. In the next section, we will analyse this H^1 -parameterization algorithm with more general features physical domains.

4 The parameterization Algorithm Analysis with Numerical Experiments

In this section, experiments are presented. The first one is a four leaf clover-shape physical domain shown in Figure 14(a). This physical domain is of complex geometric features with sharp corners and non-convex shape. The second one is a perforated model structure illustrated in Figure 14(b) with complex topology features.

For each experiment, in order to test the qualities of the resulting parameterization within IGA Framework, we will survey Jacobian of modified parameterization, the relationship between the condition number of the numerical linear system in IGA



(a) A four leaf clover-like physical domain



(b) A perforated model structure physical domain

Figure 14: The physical domains considered in Section 4

and the iteration times of Algorithm 1. For solving second order PDEs, consider the following elliptic boundary problem as a model.

$$\begin{aligned} -\Delta u &= f \\ u|_{\partial\Omega} &= 0 \end{aligned}$$

By IGA, in the weak form, the isogeometric solution is given by the solution of a numerical linear system $Ax = b$, where

$$A = [a_{i,j}]_{n \times n}, \quad (5)$$

here A is called the stiffness matrix and $a_{i,j} = \int \int_{\Omega} \nabla(B_i \circ \mathcal{P}^{-1}) \nabla(B_j \circ \mathcal{P}^{-1}) dx dy$, $\{B_i\}$ are Hermite basis functions of spline space over \mathcal{M} defined in [11], \mathcal{P} is a parameterization of Ω .

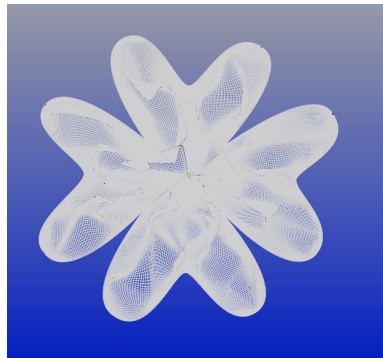
4.1 A four leaf clover-like physical domain

The initial parameterization is given in Figure 15(a). In Figure 15(b), the layout of the position of vertices of this initial parameterization is presented.

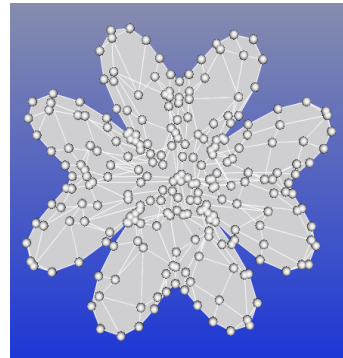
For Algorithm 1, take $\epsilon_0 = 0.001$, $\Delta t = 0.1$, $k = 1$ and $\mu = 0.001$. For this experiment, Algorithm 1 converges. With the help of Algorithm 2, the resulting parameterization is given in Figure 16(a). And in Figure 16(b), the layout of new positions of vertices is shown.

In Figures 17(a) and 17(b), Jacobians of the initial parameterization and the resulting parameterization are presented.

In order to survey the condition number of the stiffness matrix, under the same parameters, Figure 18 presents the relationship between the iteration number of

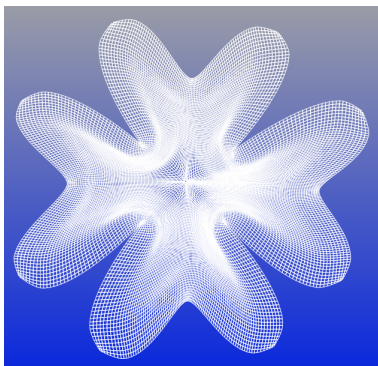


(a) The initial parameterization of the four leaf clover-like shape

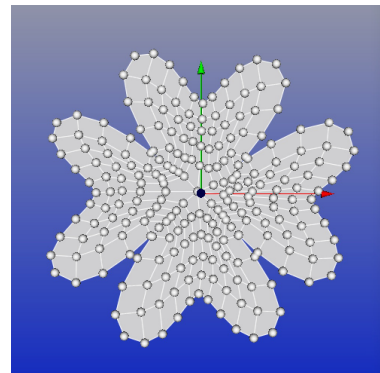


(b) The layout of the position of vertices

Figure 15: The initial parameterization and its layout of the vertex positions

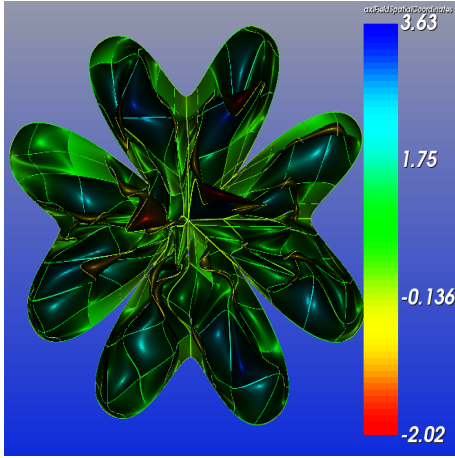


(a) The resulting parameterization of the four leaf clover-like shape

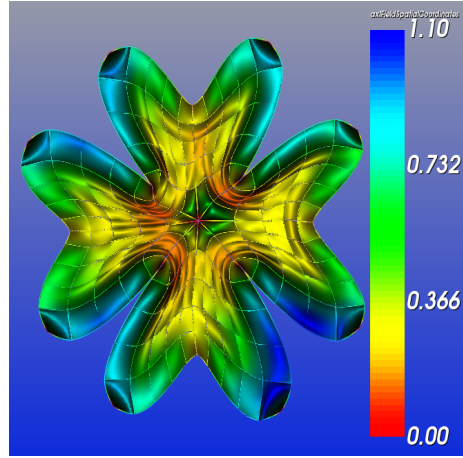


(b) The layout of the position of vertices

Figure 16: The resulting parameterization and its layout of the position of vertices



(a) The Jacobian distribution of the initial parameterization



(b) The Jacobian distribution of the resulting parameterization

Figure 17: Comparing of the Jacobians of initial parameterization and the resulting parameterization

Algorithm 1 and the natural logarithm of condition number of the stiffness matrix under the resulting parameterization with the given iteration number.

4.2 A perforated model structure physical domain

With the same structure of Section 4.1, in this section, we will take a perforated model structure as an example. The initial parameterization is given in Figure 19(a). In Figure 19(b), the layout of the position of vertices under this initial parameterization is presented.

For Algorithm 1, take $\epsilon_0 = 0.001$, $\Delta t = 0.1$, $k = 1$ and $\mu = 0.001$. Algorithm 1 converges. With the help of Algorithm 2, the resulting parameterization is shown in Figure 20(a). And in Figure 20(b), the layout of new positions of vertices is shown. Compare Jacobians of the initial parameterization and the resulting parameterization in Figures 21(a) and 21(b).

In order to survey the condition number of the stiffness matrix, under the same parameters, Figure 22 presents the relationship between the iteration number of Algorithm 1 and the natural logarithm of the condition number of the stiffness matrix under the resulting parameterization with the corresponding iteration number.

5 Conclusion and future work

This paper presents a method for modifying an initial parameterization with fixed boundaries over complex plane physical domains. Bi-cubic splines with rigid tran-

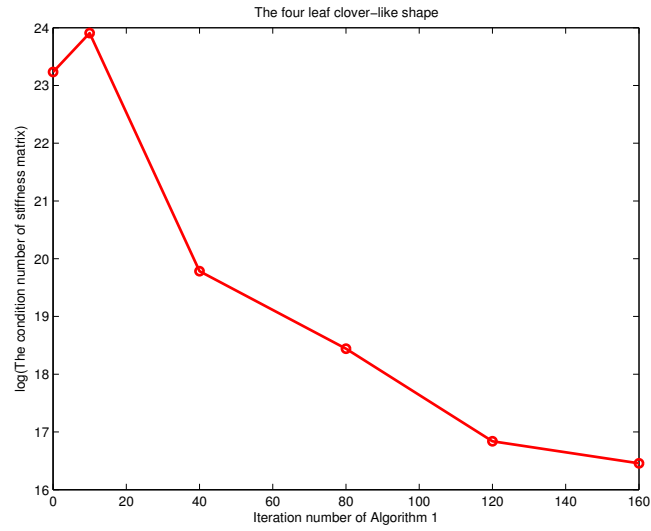
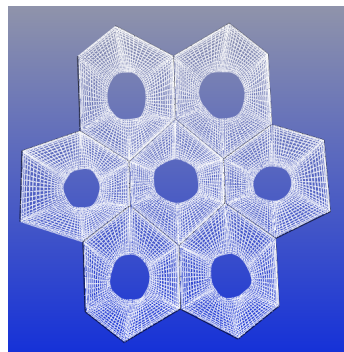
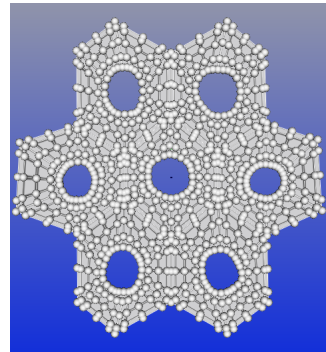


Figure 18: The relationship between the iteration number of Algorithm 1 and the condition number of stiffness matrix (Its natural logarithm)

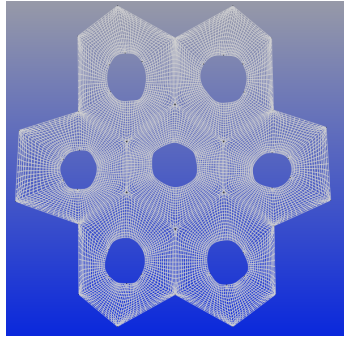


(a) The initial parameterization of the perforated model structure

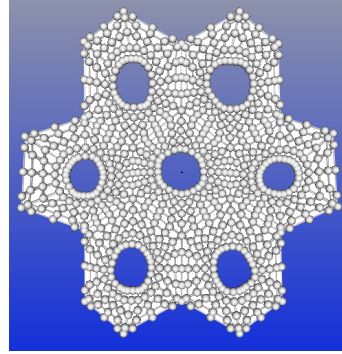


(b) Its layout of the position of the vertices

Figure 19: The initial parameterization and its layout of the position of vertices

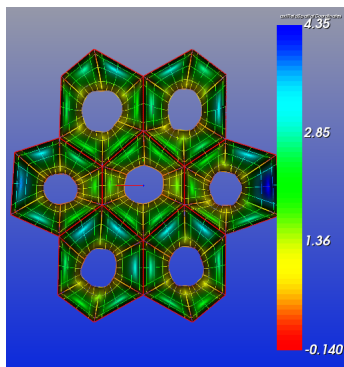


(a) The resulting parameterization of the perforated model structure

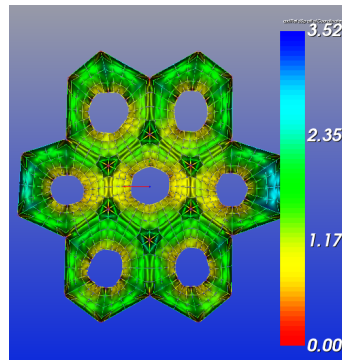


(b) Its layout of the position of vertices

Figure 20: The resulting parameterization and its layout of the position of vertices



(a) The Jacobian distribution of the initial parameterization



(b) The Jacobian distribution of the resulting parameterization

Figure 21: Comparing the Jacobians of the initial parameterization and the resulting parameterization

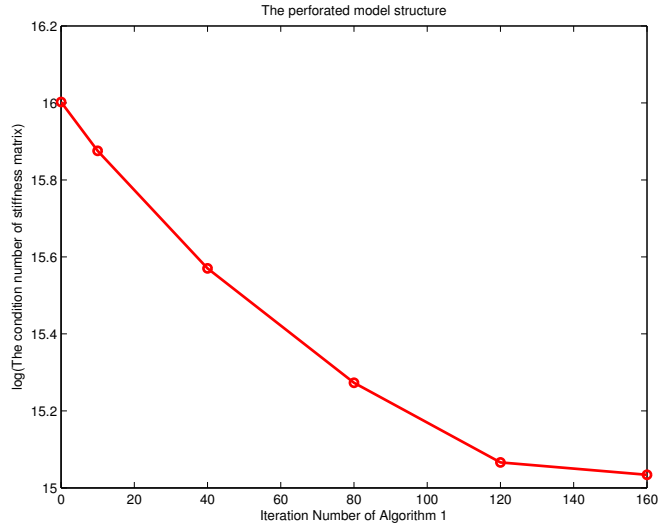


Figure 22: The relationship between the iteration number of Algorithm 1 and the natural logarithm of the condition number of stiffness matrix

sition maps in [11] are used to represent complex physical domains globally. The designing of generating parameterization algorithm is based on the three basic requirements, i.e., injective parameterization (ref. Theorem 3.2), the efficiency and numerical stability (ref. Figures 18 and 22) and the regularity property of test functions (ref. Theorem 3.2).

Within IGA, for a better solution of a second order PDE over a complex physical domain, besides the parameterization algorithm shown in this paper, an algorithm should be developed to obtain better boundaries representation for a better approximation original physical domains in the future.

6 Appendix

In this section, the proofs of lemmas and theorem are presented.

6.1 Splines in [11] and the proofs of Lemma 2.1 and Theorem 3.2

Let \mathcal{P} be a parameterization defined over a parametric mesh \mathcal{M} and $\mathcal{P} = \mathcal{P}_p + \mathcal{P}_t$, where \mathcal{P}_p is the position part of \mathcal{P} and \mathcal{P}_t is the tangent part of \mathcal{P} .

Suppose that $C = [0, 1] \times [0, 1]$ be a cell of \mathcal{M} with $v_1(0, 0), v_2(1, 0), v_3(1, 1), v_4(0, 1)$ as its vertices. Let P_1, P_2, P_3, P_4 be the position of these vertices with the help of

\mathcal{P}_p , then, over C , \mathcal{P}_p is a bicubic polynomial with vector coefficients, i. e.,

$$\mathcal{P}_p|_C(s, t) = \overrightarrow{OP_1}h_0(s)h_0(t) + \overrightarrow{OP_2}h_1(s)h_0(t) + \overrightarrow{OP_3}h_1(s)h_1(t) + \overrightarrow{OP_4}h_0(s)h_1(t), \quad (6)$$

where, $h_0(s) = (1 + 2s)(1 - s)^2$, $h_1(s) = s^2(3 - 2s)$.

Now we can prove **Lemmas 2.1**:

Proof. Suppose $\overrightarrow{OP_i} = (x_i, y_i)$, $i = 1, 2, 3, 4$. Then,

$$\mathcal{P}_p|_C(s, t) = (x(s, t), y(s, t));$$

where, $x(s, t) = \sum_{i=1}^4 x_i B_i(s, t)$, $y(s, t) = \sum_{i=1}^4 y_i B_i(s, t)$. Thus,

$$\frac{\partial x}{\partial s}(0, t) = 0; \frac{\partial x}{\partial s}(1, t) = 0; \frac{\partial x}{\partial t}(s, 0) = 0; \frac{\partial x}{\partial t}(s, 1) = 0;$$

$$\frac{\partial y}{\partial s}(0, t) = 0; \frac{\partial y}{\partial s}(1, t) = 0; \frac{\partial y}{\partial t}(s, 0) = 0; \frac{\partial y}{\partial t}(s, 1) = 0;$$

Then Jacobians along the mesh lines,

$$\mathcal{J}(0, t) = \begin{vmatrix} \frac{\partial x}{\partial s}(0, t) & \frac{\partial x}{\partial t}(0, t) \\ \frac{\partial y}{\partial s}(0, t) & \frac{\partial y}{\partial t}(0, t) \end{vmatrix} = 0; \quad \mathcal{J}(1, t) = \begin{vmatrix} \frac{\partial x}{\partial s}(1, t) & \frac{\partial x}{\partial t}(1, t) \\ \frac{\partial y}{\partial s}(1, t) & \frac{\partial y}{\partial t}(1, t) \end{vmatrix} = 0;$$

$$\mathcal{J}(s, 0) = \begin{vmatrix} \frac{\partial x}{\partial s}(s, 0) & \frac{\partial x}{\partial t}(s, 0) \\ \frac{\partial y}{\partial s}(s, 0) & \frac{\partial y}{\partial t}(s, 0) \end{vmatrix} = 0; \quad \mathcal{J}(s, 1) = \begin{vmatrix} \frac{\partial x}{\partial s}(s, 1) & \frac{\partial x}{\partial t}(s, 1) \\ \frac{\partial y}{\partial s}(s, 1) & \frac{\partial y}{\partial t}(s, 1) \end{vmatrix} = 0.$$

□

Now we can prove **Theorem 3.2**.

Proof. Denote $\mathbf{P}_i = \overrightarrow{OP_i}$, where O is the origin of the plane of the physical domain.

Case 1: If v_1, v_2, v_3, v_4 are regular vertices of \mathcal{M} ,

$$\mathcal{P}|_C(s, t) = \mathbf{T}(s, t) = \sum_{i,j=0}^3 C_{i,j} B_i^{(4)}(s) B_j^{(4)}(t),$$

where $C = (C_{i,j})_{i,j=0}^3 =$

$$\begin{pmatrix} \mathbf{P}_1 & \frac{1}{3}\mathbf{P}_2 + \frac{2}{3}\mathbf{P}_1 & \frac{2}{3}\mathbf{P}_2 + \frac{1}{3}\mathbf{P}_1 & \mathbf{P}_2 \\ \frac{2}{3}\mathbf{P}_1 + \frac{1}{3}\mathbf{P}_4 & \frac{1}{3}\mathbf{P}_1 + \frac{1}{3}\mathbf{P}_2 + \frac{1}{3}\mathbf{P}_4 & \frac{1}{3}\mathbf{P}_1 + \frac{1}{3}\mathbf{P}_2 + \frac{1}{3}\mathbf{P}_3 & \frac{2}{3}\mathbf{P}_2 + \frac{1}{3}\mathbf{P}_3 \\ \frac{1}{3}\mathbf{P}_1 + \frac{2}{3}\mathbf{P}_4 & \frac{1}{3}\mathbf{P}_1 + \frac{1}{3}\mathbf{P}_3 + \frac{1}{3}\mathbf{P}_4 & \frac{1}{3}\mathbf{P}_2 + \frac{1}{3}\mathbf{P}_3 + \frac{1}{3}\mathbf{P}_4 & \frac{2}{3}\mathbf{P}_3 + \frac{1}{3}\mathbf{P}_2 \\ \mathbf{P}_4 & \frac{1}{3}\mathbf{P}_3 + \frac{2}{3}\mathbf{P}_4 & \frac{2}{3}\mathbf{P}_3 + \frac{1}{3}\mathbf{P}_4 & \mathbf{P}_3 \end{pmatrix}$$

And,

$$\frac{\partial \mathbf{T}}{\partial s} = \frac{1}{3} \lambda_{1,1}(s, t) (\mathbf{P}_3 - \mathbf{P}_4) + \frac{1}{3} \lambda_{1,2}(s, t) (\mathbf{P}_2 - \mathbf{P}_1), \quad (7)$$

where

$$\begin{aligned} \lambda_{1,1}(s, t) &= B_3^{(4)}(t) + B_2^{(4)}(t)(B_0^{(3)}(s) + B_2^{(3)}(s)) + B_1^{(4)}(t)B_1^{(3)}(s) \geq 0; \\ \lambda_{1,2}(s, t) &= B_0^{(4)}(t) + B_1^{(4)}(t)(B_0^{(3)}(s) + B_2^{(3)}(s)) + B_2^{(4)}(t)B_1^{(3)}(s) \geq 0. \end{aligned}$$

$$\frac{\partial \mathbf{T}}{\partial t} = \frac{1}{3} \lambda_{2,1}(s, t) (\mathbf{P}_4 - \mathbf{P}_1) + \frac{1}{3} \lambda_{2,2}(s, t) (\mathbf{P}_3 - \mathbf{P}_2), \quad (8)$$

where

$$\begin{aligned} \lambda_{2,1}(s, t) &= B_0^{(4)}(s) + B_1^{(4)}(s)(B_0^{(3)}(t) + B_2^{(3)}(t)) + B_2^{(4)}(s)B_1^{(3)}(t) \geq 0; \\ \lambda_{2,2}(s, t) &= B_3^{(4)}(s) + B_2^{(4)}(s)(B_0^{(3)}(t) + B_2^{(3)}(t)) + B_1^{(4)}(s)B_1^{(3)}(t) \geq 0. \end{aligned}$$

$(\mathbf{P}_3 - \mathbf{P}_4) \times (\mathbf{P}_4 - \mathbf{P}_1)$, $(\mathbf{P}_3 - \mathbf{P}_4) \times (\mathbf{P}_3 - \mathbf{P}_2)$, $(\mathbf{P}_2 - \mathbf{P}_1) \times (\mathbf{P}_4 - \mathbf{P}_1)$ and $(\mathbf{P}_2 - \mathbf{P}_1) \times (\mathbf{P}_3 - \mathbf{P}_2)$ have the same direction. Because the quadrilateral given by P_1, P_2, P_3, P_4 is convex. Thus, the Jacobian of $\mathbf{T}(s, t)$, denoted as $\mathcal{J}(s, t)$, is positive or negative, if and only if

$$\left\| \frac{\partial \mathbf{T}}{\partial s} \times \frac{\partial \mathbf{T}}{\partial t} \right\| \neq 0.$$

Moreover,

$$\left\| \frac{\partial \mathbf{T}}{\partial s} \times \frac{\partial \mathbf{T}}{\partial t} \right\| = 0,$$

if and only if

$$\begin{cases} \lambda_{1,1}(s, t)\lambda_{2,1}(s, t) = 0; \\ \lambda_{1,1}(s, t)\lambda_{2,2}(s, t) = 0; \\ \lambda_{1,2}(s, t)\lambda_{2,1}(s, t) = 0; \\ \lambda_{1,2}(s, t)\lambda_{2,2}(s, t) = 0. \end{cases} \quad (9)$$

However, for all $(s, t) \in [0, 1] \times [0, 1]$, it does not satisfy (10). Thus, $\mathcal{J}(s, t) > 0$ (or < 0) for all $(s, t) \in C$, i.e., $\mathcal{P}|_C(s, t)$ is injective.

Based on $\mathcal{J}(s, t) > 0$ (or < 0) and the continuity of $\mathcal{P}|_C(s, t)$, locally, there exists the C^1 inverse map of $\mathcal{P}|_C(s, t)$. Thus, the image of splines on the physical domain is C^1 ($\subset H^1$).

Case 2: If v_1 is an extraordinary vertex and v_2, v_3, v_4 are regular vertices of \mathcal{M} ,

$$\mathcal{P}|_C(s, t) = \mathbf{T}(s, t) = \sum_{i,j=0}^3 C_{i,j} B_i^{(4)}(s) B_j^{(4)}(t),$$

where $C = (C_{i,j})_{i,j=0}^3 =$

$$\begin{pmatrix} \mathbf{P}_1 & \mathbf{P}_1 & \frac{2}{3}\mathbf{P}_2 + \frac{1}{3}\mathbf{P}_1 & \mathbf{P}_2 \\ \mathbf{P}_1 & \mathbf{P}_1 & \frac{1}{3}\mathbf{P}_1 + \frac{1}{3}\mathbf{P}_2 + \frac{1}{3}\mathbf{P}_3 & \frac{2}{3}\mathbf{P}_2 + \frac{1}{3}\mathbf{P}_3 \\ \frac{1}{3}\mathbf{P}_1 + \frac{2}{3}\mathbf{P}_4 & \frac{1}{3}\mathbf{P}_1 + \frac{1}{3}\mathbf{P}_3 + \frac{1}{3}\mathbf{P}_4 & \frac{1}{3}\mathbf{P}_2 + \frac{1}{3}\mathbf{P}_3 + \frac{1}{3}\mathbf{P}_4 & \frac{2}{3}\mathbf{P}_3 + \frac{1}{3}\mathbf{P}_2 \\ \mathbf{P}_4 & \frac{1}{3}\mathbf{P}_3 + \frac{2}{3}\mathbf{P}_4 & \frac{2}{3}\mathbf{P}_3 + \frac{1}{3}\mathbf{P}_4 & \mathbf{P}_3 \end{pmatrix}.$$

And,

$$\frac{\partial \mathbf{T}}{\partial s} = \frac{1}{3}\mu_{1,1}(s,t)(\mathbf{P}_3 - \mathbf{P}_4) + \frac{1}{3}\mu_{1,2}(s,t)(\mathbf{P}_2 - \mathbf{P}_1) + \frac{1}{3}\mu_{1,3}(s,t)(\mathbf{P}_3 - \mathbf{P}_1), \quad (10)$$

where,

$$\begin{aligned} \mu_{1,1}(s,t) &= B_3^{(4)}(t) + B_2^{(4)}(t)(B_0^{(3)}(s) + B_2^{(3)}(s)) \geq 0; \\ \mu_{1,2}(s,t) &= B_1^{(3)}(s)(2B_0^{(4)}(t) + B_1^{(4)}(t) + B_2^{(4)}(t)) + B_2^{(3)}(s)(B_0^{(4)}(t) + B_1^{(4)}(t)) \geq 0; \\ \mu_{1,3}(s,t) &= B_2^{(3)}(s)B_1^{(4)}(t) \geq 0. \end{aligned}$$

$$\frac{\partial \mathbf{T}}{\partial t} = \frac{1}{3}\mu_{2,1}(s,t)(\mathbf{P}_4 - \mathbf{P}_1) + \frac{1}{3}\mu_{2,2}(s,t)(\mathbf{P}_3 - \mathbf{P}_2) + \frac{1}{3}\mu_{2,3}(s,t)(\mathbf{P}_3 - \mathbf{P}_1), \quad (11)$$

where,

$$\begin{aligned} \mu_{2,1}(s,t) &= B_0^{(4)}(s)(2B_1^{(3)}(t) + B_2^{(3)}(t)) + B_1^{(4)}(s)(B_1^{(3)}(t) + B_2^{(3)}(t)) + B_2^{(4)}(s)B_1^{(3)}(t) \geq 0; \\ \mu_{2,2}(s,t) &= B_3^{(4)}(s) + B_2^{(4)}(s)(B_0^{(3)}(t) + B_2^{(3)}(t)) \geq 0; \\ \mu_{2,3}(s,t) &= B_1^{(4)}(s)B_1^{(3)}(t) \geq 0. \end{aligned}$$

Moreover, the following vectors share the same direction:

$$\begin{aligned} &(\mathbf{P}_3 - \mathbf{P}_4) \times (\mathbf{P}_4 - \mathbf{P}_1), (\mathbf{P}_3 - \mathbf{P}_4) \times (\mathbf{P}_3 - \mathbf{P}_2), (\mathbf{P}_3 - \mathbf{P}_4) \times (\mathbf{P}_3 - \mathbf{P}_1), \\ &(\mathbf{P}_2 - \mathbf{P}_1) \times (\mathbf{P}_4 - \mathbf{P}_1), (\mathbf{P}_2 - \mathbf{P}_1) \times (\mathbf{P}_3 - \mathbf{P}_2), (\mathbf{P}_2 - \mathbf{P}_1) \times (\mathbf{P}_3 - \mathbf{P}_1), \\ &(\mathbf{P}_3 - \mathbf{P}_1) \times (\mathbf{P}_4 - \mathbf{P}_1), (\mathbf{P}_3 - \mathbf{P}_1) \times (\mathbf{P}_3 - \mathbf{P}_2) \end{aligned}$$

Because the quadrilateral given by P_1, P_2, P_3, P_4 is convex. Thus, $\mathcal{J}(s,t)$ is positive or negative, if and only if

$$\left\| \frac{\partial \mathbf{T}}{\partial s} \times \frac{\partial \mathbf{T}}{\partial t} \right\| \neq 0.$$

Moreover,

$$\left\| \frac{\partial \mathbf{T}}{\partial s} \times \frac{\partial \mathbf{T}}{\partial t} \right\| = 0,$$

if and only if

$$\begin{cases} \mu_{1,1}(s,t)\mu_{2,1}(s,t) = 0; \\ \mu_{1,1}(s,t)\mu_{2,2}(s,t) = 0; \\ \mu_{1,1}(s,t)\mu_{2,3}(s,t) = 0; \\ \mu_{1,2}(s,t)\mu_{2,1}(s,t) = 0; \\ \mu_{1,2}(s,t)\mu_{2,2}(s,t) = 0; \\ \mu_{1,2}(s,t)\mu_{2,3}(s,t) = 0; \\ \mu_{1,3}(s,t)\mu_{2,1}(s,t) = 0; \\ \mu_{1,3}(s,t)\mu_{2,2}(s,t) = 0. \end{cases} \quad (12)$$

There is only one solution of (13), i.e. $(0,0) \in [0,1] \times [0,1]$. Thus,

$$\mathcal{J}(s,t) = \begin{cases} = 0, & (s,t) = (0,0); \\ > 0(\text{or } < 0), & (s,t) \neq (0,0) \end{cases}$$

i.e., $\mathcal{P}|_C(s,t)$ is injective. Because $(0,0)$ is isolated.

Now, the parameterization $\mathcal{P}|_C(s,t)$ is singular at $(0,0)$. However, the coefficients satisfy H^1 -interal assumptions when the quadrilateral given by P_1, P_2, P_3, P_4 is convex. Thus the images of splines on the physical domain are H^1 . \square

6.2 The proof of Lemma 3.1

Proof. Owing to the velocity of $P_i(t)$ at t_0 is $\mathbf{0}$,

$$\begin{aligned} P_i(t_0 + \Delta t) - P_i(t_0) &= \int_{t_0}^{t_0 + \Delta t} dt \int_{t_0}^t \frac{\mathbf{F}_i(s)}{m_i} ds \\ &= \int_{t_0}^{t_0 + \Delta t} \frac{\mathbf{F}_i(s)}{m_i} (t_0 + \Delta t - s) ds \\ &= \frac{\mathbf{F}_i(t_0 + \theta \Delta t)}{m_i} \int_{t_0}^{t_0 + \Delta t} (t_0 + \Delta t - s) ds \\ &= \frac{\mathbf{F}_i(t_0 + \theta \Delta t)}{2m_i} \Delta t^2 \end{aligned}$$

where $\theta \in [0,1]$. Thus,

$$P_i(t_0 + \Delta t) - P_i(t_0) = \frac{\mathbf{F}_i(t_0)\Delta t^2}{2m_i} + o(\Delta t^2).$$

\square

References

- [1] T. J. R. Hughes, J. A. Cottrell and Y. Bazilevs “Isogeometric analysis: CAD, finite elements, NURBS, exact geometry and mesh refinement”. *Computer Methods in Applied Mechanics and Engineering*, vol. 194, Issues. 39-41, p. 4135–4195, 2005.
- [2] E. Cohen, T. Martin, R.M. Kirby, T. Lyche, R.F. Riesenfeld. “Analysis-aware Modeling: Understanding Quality Considerations in Modeling for Isogeometric Analysis”. *Comput. Methods Appl. Mech. Engrg.* vol. 199, p. 334-356, 2010.
- [3] T. Martin, E. Cohen, M. Kirby, T. Lyche, R. Riesenfeld. “Analysis-aware modeling: quality considerations in modeling for isogeometric analysis”. *Comput. Method Appl. Mech. Engrg.* vol. 199, p. 334356, 2010.
- [4] W. Wang, Y. Zhang. “Wavelets-based NURBS simplification and fairing”. *Comput. Method Appl. Mech. Engrg.* vol. 199, p. 290300, 2010.
- [5] G. Xu, B. Mourrain, R. Duvigneau, A. Galligo. “parameterization of computational domain in isogeometric analysis: methods and comparison”. *Comput. Methods Appl. Mech. Engrg.* vol. 200, p. 2021-2031, 2011.
- [6] G. Xu, B. Mourrain, R. Duvigneau, A. Galligo. “Optimal analysis-aware parameterization of computational domain in 3D isogeometric analysis”. *Computer-Aided Design.* vol. 45, p. 812-821, 2013.
- [7] G. Xu, B. Mourrain, R. Duvigneau, A. Galligo. “Constructing analysis-suitable parameterization of computational domain from CADboundary by variational harmonic method”. *Journal of Computational Physics.* vol. 252, p. 275-289, 2013.
- [8] E. Pilgerstorfer, B. Jüttler . “Bounding the influence of domain parameterization and knot spacing on numerical stability in Iso-geometric Analysis”. *Computer Methods in Applied Mechanics and Engineering*, vol. 268, p. 589-613, 2014.
- [9] K. Gahalaut, S. Tomar. “Condition number estimates for matrices arising in the isogeometric discretizations”. *RICAM report 2012-23*, p. 138, 2012.
- [10] Hyun-Jung Kim, Yu-Deok Seo, and Sung-Kie Youn. “Isogeometric analysis with trimming technique for problems of arbitrary complex topology”. *Computer Methods in Applied Mechanics and Engineering.* vol. 199, p. 2796-2812, 2010.
- [11] M. Wu, B. Mourrain, A. Galligo, B. Nkonga. “Spline spaces over rectangular meshes with arbitrary topologies and its application to the Grad-Shafranov equation”. *submitted to Comput. Methods Appl. Mech. Engrg.*

- [12] S. Lipton, J.A. Evans, Y. Bazilevs, T. Elguedj, T.J.R. Hughes. “Robustness of isogeometric structural discretizations under severe mesh distortion”. *Comput. Methods Appl. Mech. Engrg.* vol. 199, p. 357-373, 2010.
- [13] T. Kamada, S. Kawai. “An algorithm for drawing general undirected graphs”. *Information Processing Letters.* vol. 31, p. 7-15, 1989.
- [14] B. Becker, G. Hotz. “On the optimal layout of planar graphs with fixed boundary”. *SIAM J. Comput.* vol. 16, p. 946-972, 1987.
- [15] V.M. Calo, H. Gómez, Y. Bazilevs, G.P. Johnson, T.J.R. Hughes, “Simulation of Engineering Applications Using Isogeometric Analysis”. *Proceedings of Tera Grid.* 2008.
- [16] W. T. Tutte, “How to draw a graph”. *Proc. London Math. Society.* vol. 13, p. 743-768, 1963.
- [17] P. Eades, “A heuristic for graph drawing”. *Congressus Numerantium.* vol. 42, p. 149-160, 1984.
- [18] J. Joseph Fowler, Stephen G. Kobourov, “Planar Preprocessing for Spring Embedders.” *Graph Drawing.* p: 388-399, 2012.
- [19] T. Takacs, B. Jüttler. “Existence of Stiffness Matrix Integrals for Singularly Parameterized Domains in Isogeometric Analysis”. *Computer Methods in Applied Mechanics and Engineering,* vol. 200, p. 3568–3582, 2011.
- [20] T. Takacs, B. Jüttler. “ H^2 regularity properties of singular parameterizations in isogeometric analysis”. *Graphical Models,* vol. 74, p. 361–372, 2012.